Mon. Not. R. Astron. Soc. **000**, 000–000 (0000) Printed 6 November 2013 (MN LATEX style file v2.2)

# Cosmic web correlations with the shape, spin and peculiar velocties of dark matter halos

Sergio Contreras[1] Jaime E. Forero-Romero[1] Nelson Padilla[1]

[1] *Uni A* [2] *Uni B*

6 November 2013

**ABSTRACT**

We study the alignment of DM halos with the cosmic web as described by the tidal and velocity shear fields. We focus on the alignment of halos shape, spin and peculiar velocities. We use a cosmological N-body simulation that allows to study dark matter halos spanning four orders of magnitude in mass ((10$^{10}$-10$^{14}$) $h^{-1}$M$_\odot$and spatial scales of (0.5-1.0)$h^{-1}$Mpc to define the cosmic web. After varying the numerical parameters in our experiments we find that the tidal field provides a robust description for the different kinds of alignments. We measure a strong here is a strong alignment of the peculiar velocity field and the halo shape with the cosmic web defined by the tidal field. The results for the spin alignment are less significant. The shape alignment is stronger for halos that are either massive ($M > 10^{12}h^{-1}$M$_\odot$), have large or are located in high density regions.

**Key words:** methods: N-body simulations, galaxies: haloes, cosmology: theory, dark matter, large-scale structure of Universe

## 1 INTRODUCTION

The formation of large scale structure in the Universe proceeds by gravitational instability. This is an intrinsic anisotropic process. [Pancake formation ...]

Numerical simulations allow the exploration of a deep nonlinear regime, following the formation of virialized dark matter halos, which host observable galaxies. Some characteristics of these halos have to be linked to the environment in which they formed. One way to studty the connection halo-environment is to quantify the degree of correlation between different halo properties and their surrounding density and velocity fields.

Among the properties that are of interest we find the shape, spin and peculiar velocity. [Relevanc of dark matter halo shapes ...] [Relevance of halo spin ...] [Relevance of peculiar velocities]

There is large tradition of theoretical precedents for the measurements of shape and spin alignment. In this paper we review most of these studyes and offer our own study with complementary numerical techniques and simulations. [Brief summary of the appendix ...]

We also present the results for the alignment of peculiar velocities with large scale structure. Such a study has received less atention in the literature. However, we consider that it presents relevant insights for the study of cosmic flows.

The structure of this paper is the following.

Author Web Method Halo Finder Major Axis Correlation SHAPE

## 2 THEORETICAL PRECEDENTS

... There is abundant literature on the issue of shape and angular momentum aligmnent of dark matter haloe with respect to the cosmic we.

... This alignment is often measured from the distribution of the $\cos\theta$ where $\theta$ is the angle between the two axes of interest.

... Table 1 and Table 2 summarizes recent results found in the literature for shape and angular momentum alignment.

The tidal connection between voids in simulations (Platen et al. 2008), the alignment of observed galaxies with the inferred tidal field(Lee & Erdogdu 2007; Jones et al. 2010). There are other kind of alignment statistics based on modifications of the correlation (Paz et al. 2008; Faltenbacher et al. 2009) that go beyond a local computation and therefore are not reviewed in detail in this paper.

## 3 N-BODY SIMULATION AND HALO FINDING

In this paper we use the Bolshoi simulation that follows the non-linear evolution of a dark matter density field on cosmological scales. The volume is a cubic box with 250$h^{-1}$Mpc on

| Author | Web Method | Spatial Scale | Along | Alignment | Mass dependence |
|---|---|---|---|---|---|
| **Contreras et al. (2014)** | T-Web | $0.5-1h^{-1}$Mpc | filament | ? | $>10^{12}h^{-1}\mathrm{M}_{\odot}$ |
| | | | filament | ? | $<10^{12}h^{-1}\mathrm{M}_{\odot}$ |
| | | | wall | ? | all masses |
| **Contreras et al. (2014)** | Vp-Web | $0.5-1h^{-1}$Mpc | filament | ? | $>10^{12}h^{-1}\mathrm{M}_{\odot}$ |
| | | | filament | ? | $<10^{12}h^{-1}\mathrm{M}_{\odot}$ |
| | | | wall | ? | all masses |
| Libeskind et al. (2013) | V-Web | $1h^{-1}$Mpc | filament | ++ | $>10^{12}h^{-1}\mathrm{M}_{\odot}$ |
| | | | filament | + | $<10^{12}h^{-1}\mathrm{M}_{\odot}$ |
| | | | wall | ++ | all masses |
| Zhang et al. (2009) | Hessian density field | $2.1h^{-1}$Mpc | filament | ++ | $>10^{12}h^{-1}\mathrm{M}_{\odot}$ |
| | | | filament | + | $<10^{12}h^{-1}\mathrm{M}_{\odot}$ |
| Aragón-Calvo et al. (2007) | Hessian density field | - | wall | ++ | $>10^{12}h^{-1}\mathrm{M}_{\odot}$ |
| | | - | wall | + | $<10^{12}h^{-1}\mathrm{M}_{\odot}$ |
| | | - | filament | ++ | $>10^{12}h^{-1}\mathrm{M}_{\odot}$ |
| | | - | filament | + | $<10^{12}h^{-1}\mathrm{M}_{\odot}$ |

**Table 1.** Shape alignment with the cosmic web. Summary of theoretical results provided by methods comparable to ours.

| Author | Web Method | Spatial Scale | Along | Alignment | Mass dependence |
|---|---|---|---|---|---|
| **Contreras et al. (2014)** | V-Web | $1h^{-1}$Mpc | filament | ? | $>10^{12}h^{-1}\mathrm{M}_{\odot}$ |
| | | | filament | ? | $<10^{12}h^{-1}\mathrm{M}_{\odot}$ |
| | | | wall | ? | all masses |
| **Contreras et al. (2014)** | Vp-Web | $1h^{-1}$Mpc | filament | ? | $>10^{12}h^{-1}\mathrm{M}_{\odot}$ |
| | | | filament | ? | $<10^{12}h^{-1}\mathrm{M}_{\odot}$ |
| | | | wall | ? | all masses |
| Libeskind et al. (2013) | V-Web | $1h^{-1}$Mpc | filament | − | $>10^{12}h^{-1}\mathrm{M}_{\odot}$ |
| | | | filament | + | $<10^{12}h^{-1}\mathrm{M}_{\odot}$ |
| | | | wall | ++ | all masses |
| Trowland et al. (2013) | Hessian density | $2-5h^{-1}$Mpc | filament | − | $>5\times10^{12}h^{-1}\mathrm{M}_{\odot}$ |
| | | | filament | + | $<5\times10^{12}h^{-1}\mathrm{M}_{\odot}$ |
| Codis et al. (2012) | Morse Theory & Tidal Web | $1-5h^{-1}$Mpc | filament | −− | $>10^{12}h^{-1}\mathrm{M}_{\odot}$ |
| | | | filament | ++ | $<10^{12}h^{-1}\mathrm{M}_{\odot}$ |
| | | | wall | ++ | all masses |
| Zhang et al. (2009) | Hessian density field | $2.1h^{-1}$Mpc | filament | ++ | only if anticorrelated with shape |
| | | | filament | −− | only if correlated with shape |
| Aragón-Calvo et al. (2007) | Hessian density field | - | wall | ++ | $>10^{12}h^{-1}\mathrm{M}_{\odot}$ |
| | | - | wall | + | $<10^{12}h^{-1}\mathrm{M}_{\odot}$ |
| | | - | filament | − | $>10^{12}h^{-1}\mathrm{M}_{\odot}$ |
| | | - | filament | + | $<10^{12}h^{-1}\mathrm{M}_{\odot}$ |
| Hahn et al. (2007) | Tidal Web | $2.1h^{-1}$Mpc | filament | − | none |
| | | $2.1h^{-1}$Mpc | wall | ++ | stronger $>10^{12}h^{-1}\mathrm{M}_{\odot}$ |

**Table 2.** Spin alignment with the cosmic web. Summary of theoretical results provided by methods comparable to ours.

a side, the matter density field is sampled with $2048^3$ particles. The cosmological parameters in the simulation correspond to the results inferred from WMAP5 data, which are also consistent with the more recent results of WMAP9. These parameters are $\Omega_m = 0.27$, $\Omega_\Lambda = 0.73$, $\sigma_8 = 0.82$, $n_s = 0.95$ and $h = 0.70$ for the matter density, cosmological constant, normalization of the power spectrum, the slope in the spectrum of the primordial matter fluctuation and the dimensionless Hubble constant. With this conditions the mass of each dark matter particle in the simulation corresponds to $m_p = 1.4\times10^8 h^{-1}\mathrm{M}_{\odot}$.

In this paper we use groups found with a Friends-Of-Friends (FOF) halo finder using a linking length of $b = 0.17$ times the mean interparticle separation. This choice translates into halos with a density of 570 times the mean density at $z = 0$. The measurements for the shape, angular momentum and peculiar velocity are done using the set of particles in each dark matter halo. The definition we use in this

paper for the shape comes from the diagonalization of the reduced inertia tensor.

$$\mathcal{T}_{lm} = \sum_i \frac{x_{i,l} x_{i,m}}{R_i^2}, \quad (1)$$

where $i$ is the particle index in the halo and $l, m$ run over the three spatial indexes and $R_i^2 = x_{i,1}^2 + x_{i,2}^2 + x_{i,3}^2$, where the positions are measured with respect to the center of mass.

The spin is calculated as

$$\vec{J} = \sum_i m_p R_i \vec{v}_i, \quad (2)$$

where the velocities are also measured with respect to the center of mass velocity. Finally the peculiar velocity of a halo is computed as the center of mass velocity.

## 4 THE COSMIC WEB ALGORITHMS

We use two algorithms to define the cosmic web on cosmological N-body simulations. Both are based on the same algorithmic principle, which is determining locally a symmetric tensor which can be diagonalized to yield three real eigenvalues $\lambda_1 > \lambda_2 > \lambda_3$ and their corresponding eigenvectors $\mathbf{e}_1$, $\mathbf{e}_2$ and $\mathbf{e}_3$. This allows for a local classification into one of the following four categories: void, sheet, filament and peak depending whether the number of eigenvalues larger than a given threshold $\lambda_{th}$ is 3, 2, 1 or 0, respectively.

We use two different symmetric tensors. The first is the shear tensor, defined as the hessian of the gravitational potential, normalized in such a way as to be dimensionless:

$$T_{\alpha\beta} = \frac{\partial^2 \phi}{\partial r_\alpha \partial r_\beta}, \quad (3)$$

where $\phi$ is the gravitational potential rescaled by a factor $4\pi G\bar{\rho} = 3/2\Omega_m H_0^2$ in such a way that the Poission equation can be written as:

$$\nabla^2 \phi = \delta, \quad (4)$$

where $\delta$ is the matter overdensity, $\bar{\rho}$ is the average matter density, $H_0$ is the Hubble constant at present time and $\Omega_m$ is the matter density parameter.

The second tensor is the velocity shear:

$$\Sigma_{\alpha\beta} = -\frac{1}{2H_0}\left(\frac{\partial v_\alpha}{\partial r_\beta} + \frac{\partial v_\beta}{\partial r_\alpha}\right) \quad (5)$$

### 4.1 Numerical considerations

In this paper we compute the cosmic web on grids of two different resolutions $256^3$ and $512^3$. In the case for the Tweb we interpolate

## 5 RESULTS

### 5.1 Interweb Alignment

In the first place we wish to directly compare the results of the two algorithms. For the two algorithms we have the information for the eigenvectors and the eigenvalues on exactly the same positions defined by the grids. This allows us to-compute the pair-wise allignment between the eigenvectors in the two web finders.

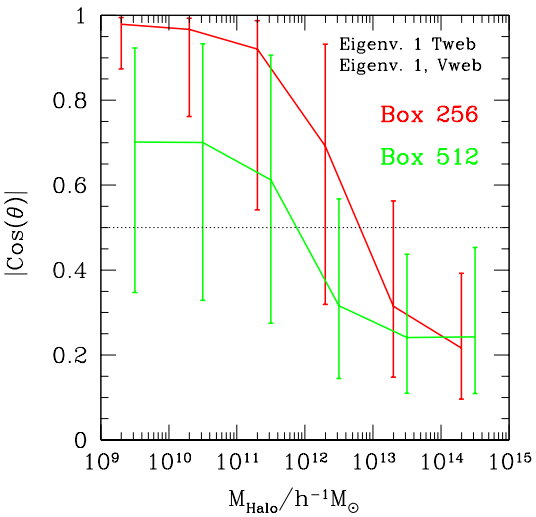


**Figure 1.** Median of the interweb alignment for the two grid resolutions as a function of the dark matter mass corresponding to the halos where the measurement was made. The error bars indicate the lower and upper quartiles (Figure in color in the web version).

We are mainly interested in the alginment of the web with the halos. Therefore we restrict our analysis to the grid cells that are occupied by halos. If we had decided to perform this kind of analysis on all the grid cells, the statistics would be dominated by the void regions, because the dominate in number the fraction of cells in the simuation.

Figure 1 shows the results of the inter-web alignment as a function of halo mass. It clearly stands out that the eigenvectors are aligned for low mass halos but are close perpendicular to each other at the location of the most massive halos. There is a transition scale around $(10^{11.5} - 10^{12.5})h^{-1}\mathrm{M}_\odot$depending on the grid resolution. The coarse grid $(256^3)$shows the transition at higher masses than the fine grid $(512^3)$.

For both resolutions, the halos more massiven than $10^{13}h^{-1}\mathrm{M}_\odot$are locate in regions where the fastest momentum-weighted collapse direction (defined by the V-web) is perpendicular to the direction where the tidal compression is the highest.

The fact that this trend is less evident at low resolution and low masses, hints that the flip is actually related to the overdensity values, i.e. to the degree of non-linearity, in the corresponding spatial scales.

### 5.2 Shape Alignment

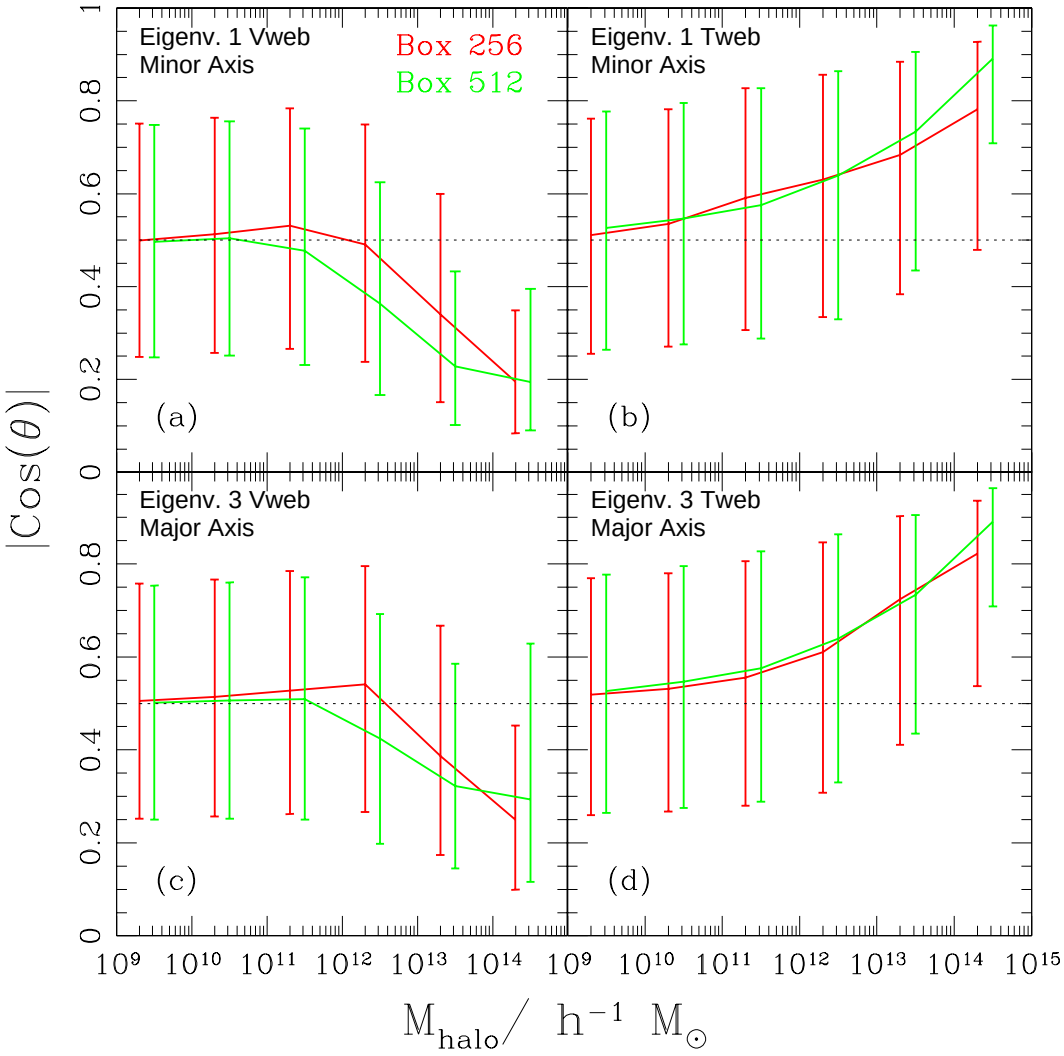


**Figure 2.** Median of $\cos\theta$ quantifying the shape alignment for the Vweb (left) and the Tweb (right) at two different grid resolutions. In the upper (lower) panels the angle $\theta$ is measured between the halo minor (major) axis and the first (third) eigenvector.

### 5.3 Angular Momentum Alignment

### 5.4 Peculiar velocity Alignment

Possible conclusion. Prolateness follow concentration. In the Tweb Angular momentum alignment is influenced by spin at higher masses. In the Vweb angular momentum alginment is influenced by all factors. In the peculiar velocity alginment only spin seemss to have an effect.

### 5.5 What drives the alignment

We wish to understand what other selection criteria on halo properties can produce a stronger local alignment for the shape, spin and peculiar velocities. We split the halo population into low and high mass halos imposing a cut at $M_{\rm halo} = 10^{11}h^{-1}{\rm M}_{\odot}$. This allows us to have robust statistics on the high mass end. We have also computed these results for a cut at $M_{\rm halo} = 10^{12}h^{-1}{\rm M}_{\odot}$and checked that the results we report below are not affected by this change.

For each mass interval we perform cuts in the following properties: spin, concentration, triaxiallity, circularity and density. We measure the web alignments in two sets, each one including the 30% of halos in the lower/higher end of the corresponding property.

## 6 DISCUSSION

We do not find a strong signal for the alignment of spin and the cosmic web. A significant correlation signal has been recently measured between the spin and the cosmic vorticity (**?**Laigle et al. 2013). This two facts are consistent with spin being produced by the non-symmetric part of the shear and tidal tensors.

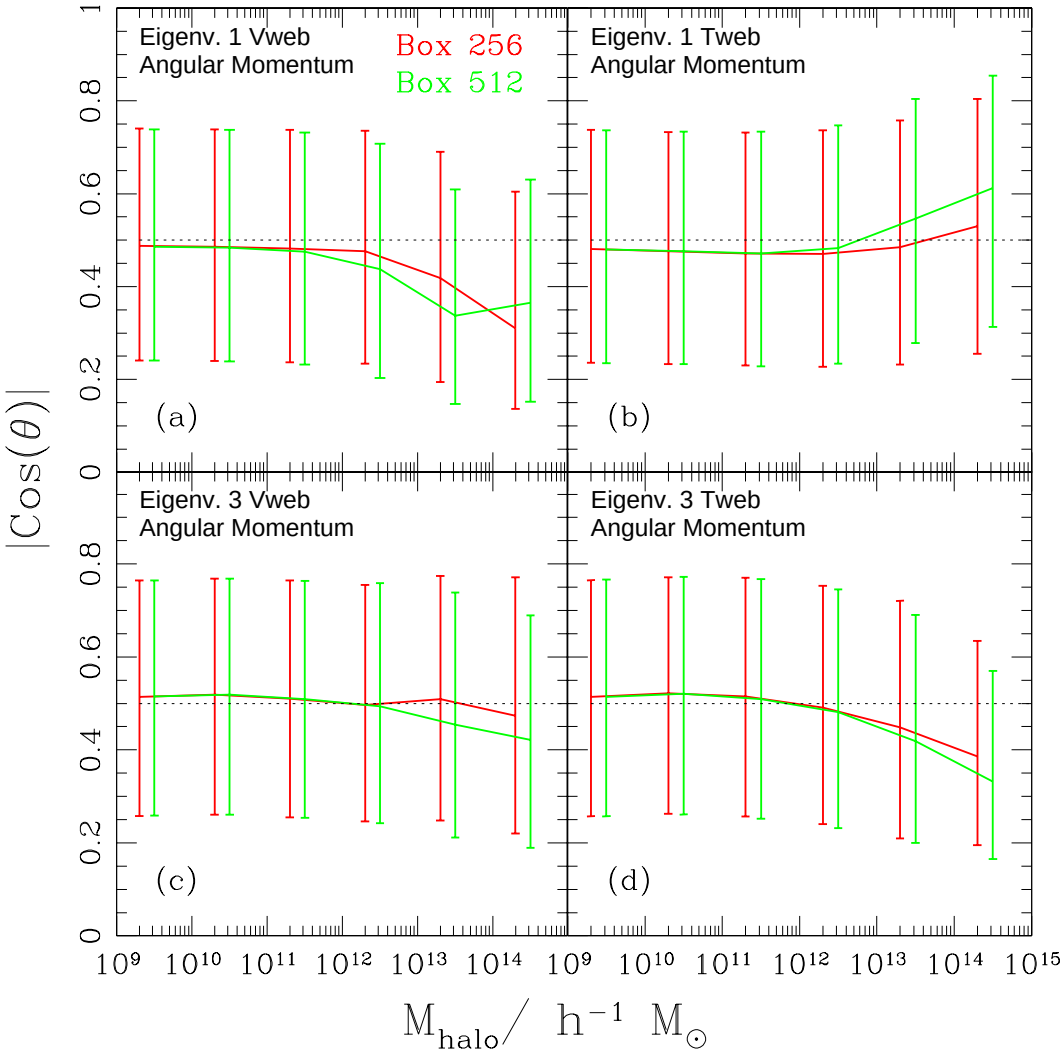


**Figure 3.** Median of $\cos\theta$ quantifying the angular momentum alingment for the Vweb (left) and the Tweb (right) at two different grid resolutions. In the upper (lower) panels the angle $\theta$ is measured between the first (third) eivenvector and the angular momentum vector.

## 7 CONCLUSIONS

## ACKNOWLEDGMENTS

## APPENDIX A. DETAILED DESCRIPTION OF PREVIOUS THEORETICAL RESULTS

• (Libeskind et al. 2013) Studies shape and spin alignment with the cosmic web defined by the velocity shear tensor method described in this paper.

The simulation has $2048^3$ particles in a box of $250h^{-1}$Mpc , corresponding to a particles mass of $1.3\times10^8h^{-1}\mathrm{M}_\odot$. Halos are found using a FOF halo finder with $b = 0.17$. The catalog only include halos more massiven than $3 \times 10^9h^{-1}\mathrm{M}_\odot$.

The shape is defined from the reduced inertia tensor. Results are reported for three mass bins $M_{\rm vir} < 10^{11.5}h^{-1}\mathrm{M}_\odot$, $11^{11.5} < M_{\rm vir} < 12^{12.5}h^{-1}\mathrm{M}_\odot$ and $M_{\rm vir} > 12^{12.5}h^{-1}\mathrm{M}_\odot$.

The identification of the cosmic web is done on a grid of $256^3$ with a gaussian smoothing of $\sim 1h^{-1}$Mpc over the velocity field. We define this velocity field as the ratio of a momentum density to the matter density field. The details of this approach are described in the Appendix .

The aligmnet signal of the spin is very weak while the shape alignment signal is very strong. The shape alignment is such that the eigenvector corresponding to the smallest eigenvalue is aligned with the major axis. This effect is stronger for more massive halos. In other words the major axis of a halo is aligned with a filament, and lies on the plane that define a sheet. However the spin is antialgined with the filament for massive halos and weakly aligned for low mass halos.

• (Trowland et al. 2013)

The simulation is the millennium run, which has $2160^3$ particles in a volume of $500h^{-1}$Mpc on a side. This corresponds to a particle mass of $8.6 \times 10^8h^{-1}\mathrm{M}_\odot$. The catalog uses both halos and subhalos which were identified with SUBFIND. Only halos with more than 500 particles were kept to get a robust computation for the spin. For each halo the spin is defined as the sum of the angular momentum of each particle with respect to the center of mass.

The method to define the filamentary structure is based on the eigenvalues of the hessian of the density.However the analysis are reported ona box of $300h^{-1}$Mpc on a side. Four

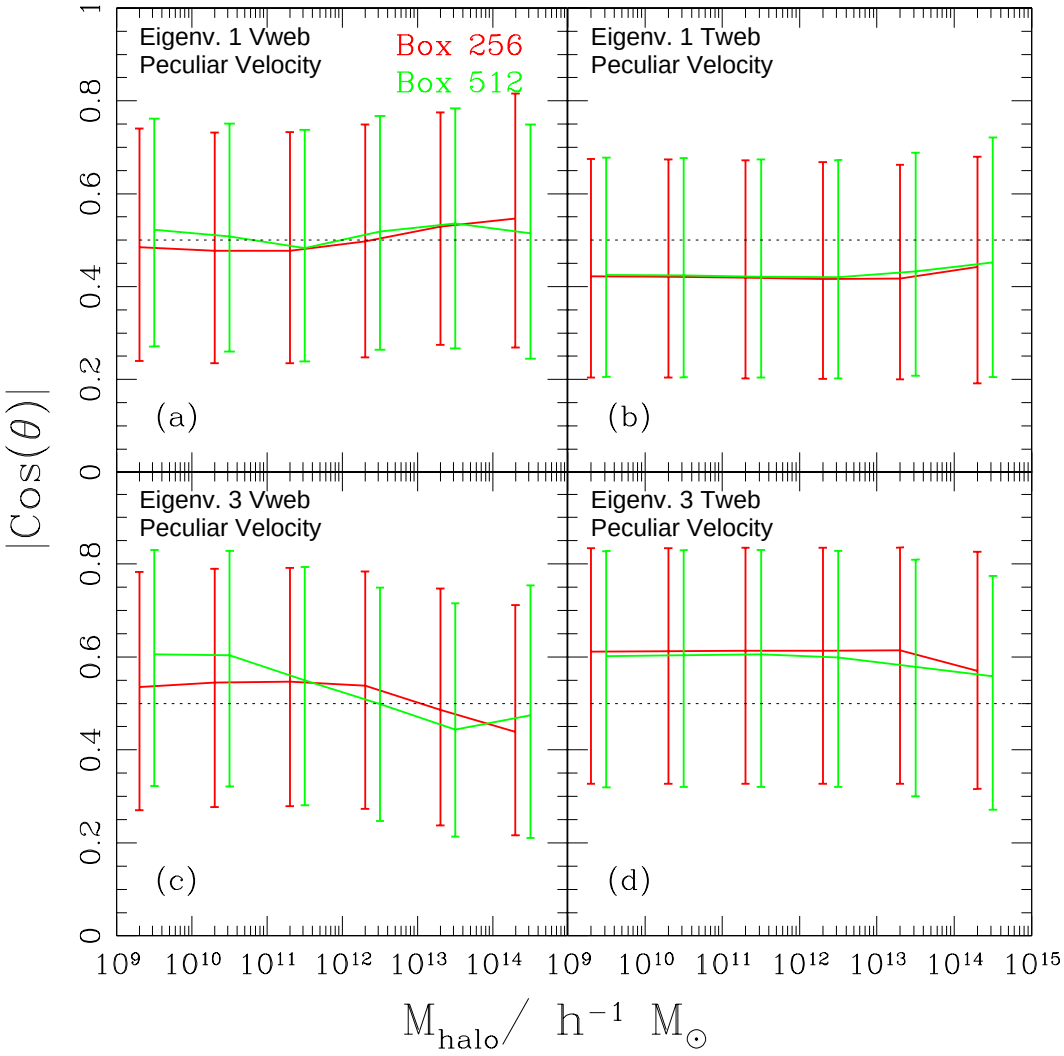


**Figure 4.** Median of $\cos\theta$ quantifying the peculiar velocity alignment with the Vweb (left) and the Tweb (right) at two different grid resolutions. In the upper (lower) panels the angle $\theta$ is measured between the first (third) eivenvector and a halo's peculiar velocity.

different gaussian smoothing scales are used: 2.0, 3.0 and $5.0h^{-1}$Mpc .

The authors report a slight alignment signal of spin against the principal filament axis. By fitting the following functional form to the $\cos(\theta)$ distribution

$$P(\cos\theta) = (1-c)\sqrt{1+\frac{c}{2}}\left[1-c\left(1-\frac{3}{2}\cos^2\theta\right)\right]^{-3/2}, \quad (6)$$

they are able to quantify the degree of alignment ($c < 0$) or antialignment ($c > 0$). This parameterization is based on theoretical expectactions of Tidal Torque Theory (TTT) (Lee et al. 2005). At $z = 0$, the reported value is $c = 0.035 \pm 0.004$, where the uncertainty was calculated using bootstraping and resampling.

When the halo sample is divided between low mass and high mass halos with a transition scale $M_\star = 5.9 \times 10^{12}\mathrm{M}_\odot$, there is an anti-alignment above this mass and an alignment below it.

- (Codis et al. 2012) Studies the alignment of the spin of dark matter halos relative to the surrounding large scale structure and to the tidal tensor eigenvalues.

They use a dark matter simulation with $4096^3$ DM particles in a cubic periodic box of $2000h^{-1}$Mpc on a side, which corresponds to a particle mass of $7.7 \times 10^9\mathrm{M}_\odot$. Halos are identified using a FoF algorithm with a linking legth of 0.2 keeping all halos with more than 40 particles, which sets the minimum halo mass to be $3 \times 10^{11}\mathrm{M}_\odot$. In their work the particles were sampled on a $2048^3$ grid and the density field was smoothed with a gaussian fileter over a scale of $5h^{-1}$Mpc corresponding to a mass of $1.9 \times 10^{14}$. The skeleton was computed over $6^3$ overlapping subcubes and then reconnected.

The filament finder algorithm is based on Morse theory and defines a Skeleton to be the set of critical lines joining the maxima of the densit field through saddle points following the gradient. They also compute the hessinan of the potential over the smoothed density field to get their eigenvectors.

The spin of the halo is defined as $m_p \sum_i (r_i - \bar{r}) \times (v_i - \bar{v})$

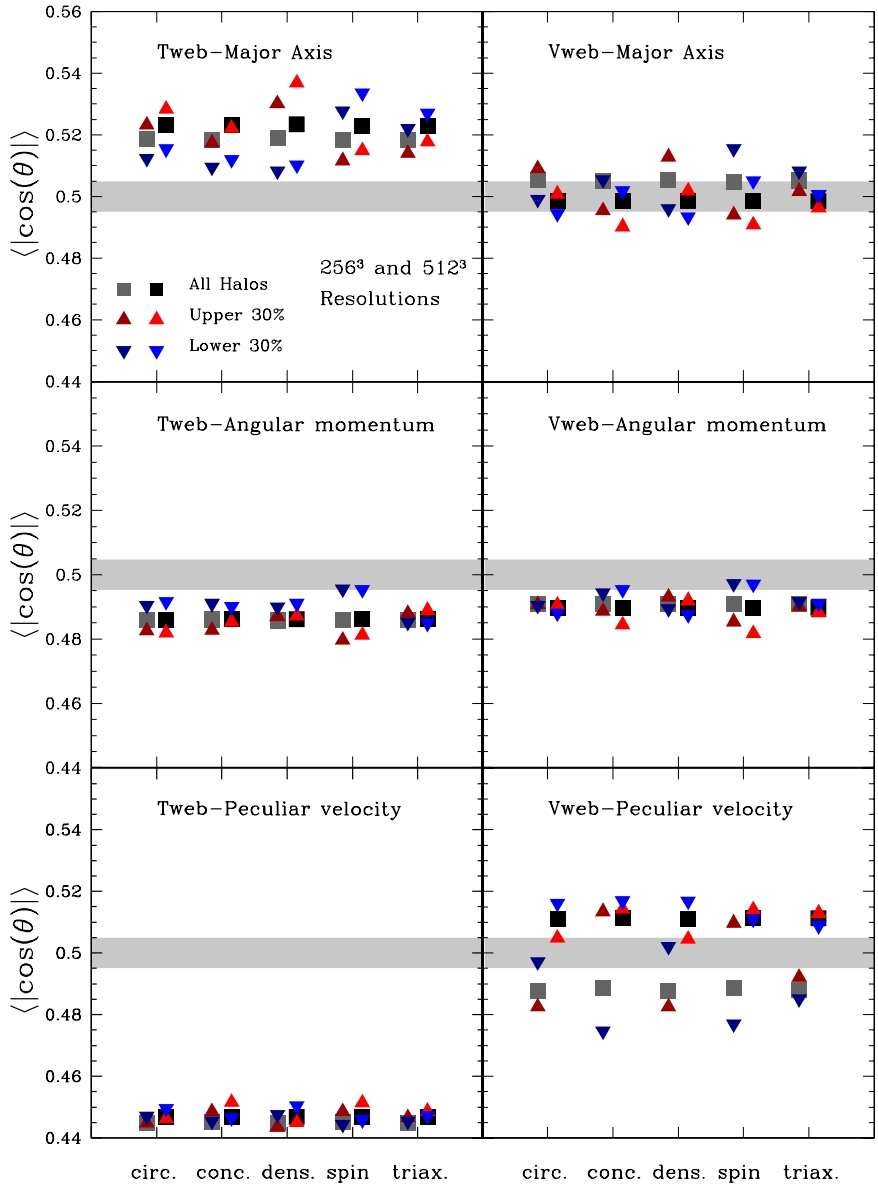


**Figure 5.** The alignment is always taken with respect to the first eigenvector.

where $\bar{r}$ is the center of mass of the halo and $\bar{v}$ is the average velocity.

They measure the sping alignment with each one of the eigenvectors. With repecto to the minor eigenvector $e_1$ there is antialignement for masses $M > 5 \times 10^{12} \mathrm{M}_{\odot}$and alignment for masses $< 5 \times 10^{12} \mathrm{M}_{\odot}$. With respect to the intermediate eigenvector $e_2$ there is a strong alignment at high masses and no alignment for low masses, with respecto the major eigenvector $e_3$ there is an anti-alignment signal at all masses. The results from the Skeleton algorithm are in perfect agreement with the results from the Tidal web. The transitional mass is weakly dependent on the smoothing scale, varing between $1 - 5 \times 10^{12} h^{-1} \mathrm{M}_{\odot}$for smoothing scales between $1.0 - 5.0 h^{-1}$Mpc .

• (Zhang et al. 2009) Study the spin and shape alignment against filaments.

They use a dark matter simulation with $1024^3$ DM particles in a periodic box of 100 $h^{-1}$Mpc on a side. The particle mass is $6.92 \times 10^7 h^{-1} \mathrm{M}_{\odot}$. Dark matter haloes are found using a FOF algorithm with a linking length of 0.2 times the interparticle distance. Only halos with more than 500 particles are retained for further analysis.

The angular momentum is measured with positions repect to the center of mass and the shape is determined using the non-normalized moment of inertia tensor.

The environment is found using the hessian of the density. The density field was interpolated over a $1024^3$ grid and then smoothed with a Gaussian filter of scale $R_s = 2.1 h^{-1}$Mpc . There are two methods to define the direction of a filament. The first method uses the eigenvalues of the hessian density, howevere they define the filament direction with the eigenvector corresponding the single positive eigenvalue of the hessian. The second method used a line that connects the two terminal halos in a filament segment.

The characterization of the alingment with the $\cos(\theta)$ statistic. For the method that uses the eigenvectors, they find that the strenght of the spin alignment decreases with halo mass. For the shape they study the alingment of the major axis with the filament. The find an alignment signal in all mass bins, with an stronger effect for more massive halos.

In a final experiment they measure the spin alignment in four different samples that separated by the strength of the shape alignment. They find that halos anticorrelated in shape, show a strong sping correlation going to the extreme where there is a strong spin anticorrelation for halos with a strong shape correlation. This means that the halos with strong spin alignment are not the same halos showing strong shape alignment.

• (Aragón-Calvo et al. 2007) The method is the Multiscale Morphology Filter which is based on the Hessian matrix of the density field, where the density field is computed from the particle distribution using a Delaunay tesselation field estimatior (DTFE), which is self-adaptive. This allows them to identify clusters, filaments and walls.

The simulation has $512^3$ particles in a cubic box of $150h^{-1}$Mpc . The mass per particle is $2 \times 10^9 h^{-1}\mathrm{M}_\odot$. Halo identitification is done with the HOP algorithm. They keep halos with more than 50 partices and less than 5000, defining a mass range of$1 - 100 \times 10^{11} h^{-1}\mathrm{M}_\odot$.

The principal axes of each halo are computed from the non-normalized inertia tensor. The inertian tensor and the angular momentum are computed with respect to the center of mass of the halo.

They compute two angles, one with respect to the direction defining the filaments and the other the walls. Their results make a distinction between halos of more massive and less massive than $10^{12} h^{-1}\mathrm{M}_\odot$.

The halo spins tend to lie on the plane of the wall. This is stronger for massive halos.The effect for filaments is weaker: low mass halos tend to lieparallel to their host filament, while high mass halos tend to be perpendicular.

Theres is a very strong effect for the principal axes of halos in filaments to be strongly correlated with the direction of the filaments. The minor axis tend to be perpendicular to the filament. This effect is stronger for larger halos.

The effect in walls is less strong ,but still the minor axis tend to lie perpendicular to the wall, while the other axis then to lie over the wall. The effect is stronger for massive halos.

They find that spins and shapes of dark matter halos are significantly correlated with each other and with the orientation of their host structures.

• (Hahn et al. 2007)The method is the Tweb. They use three simulations each of $512^3$ particles, with sizes $L_1 = 45h^{-1}$Mpc , $L_2 = 90h^{-1}$Mpc and $L_3 = 180h^{-1}$Mpc , this corresponds to particle masses of $4.7, 38.0, 300 \times 10^7 h^{-1}\mathrm{M}_\odot$. The normalization is $\sigma_8 = 0.9$. Halo identification was done with a FOF algorithm with 0.2 times the interparticle distance. They consider halos of at least 300 particles.

The web is obtained for a grid of $1024^3$ cells, the density field is obtained with a CIC interpolation and smoothed using a Gaussian Kernel. In the rest of the paper all the results correspond to a smoothing scale of $R_s = 2.1h^{-1}$Mpc .

They Report on the angle between the halo angular momentum vector and the eigenvector corresponding to perpendicular directions to the sheets and the direction of the filaments. This is divided in two halo populations: $5 \times 10^{10} - 1.0 \times 10^{12}$ and $> 10^{12}$. There is a weak antialignment in the case of the filaments and a stronger antialignment in the case of the sheets. For the sheets the effect is stronger for the massive bin. In the filaments the alignment is weak regardless of the mass. They do not report any other significan statistic, but recognize that they suffer from small-number statistics in voids).

They do not see any strong dependance of the environment in the shape. They do not measure the shape alinment.

• (Brunino et al. 2007) Uses a DM only N-body simulation (the Millennium Run) to study the shape and angular momentum alignment with respect to large cosmological voids.

The voids are found with a spherical void finder. This algorithm first looks for potential void centers in the underdense regions of the simulation. These positions define the centers of spheres that are empty of halos above a given mass threshold. Only voids with radius larger than $10h^{-1}$Mpc were considered for further analysis.

Halos were identified by linking particles with density exceeding 900 times the background density in order to keep the analysis of shape and angular momentum on the core of the halo. Only halos with masses in the range $8.6 \times 10^{11} h^{-1}\mathrm{M}_\odot < M_\mathrm{h} < 8.6 \times 10^{12} h^{-1}\mathrm{M}_\odot$ were included analized to measure their angular momentum and the inertia tensor, both in a non-normalized way.

For the purpose of measuring alignments a second cut is imposed whereby only halos within a shell of radius $R_{void} < r < 1.05R_{void}$. The alignment is then measured between the vector connecting the center of the void to the halo in question and the vector of interest.

The results show that there is a strong alignment of halo shape in such a way that the major axis is parallel to the shell surrounding the void. In the case of angular momentum there is not a significant signal for alignment.

• (Basilakos et al. 2006) Use a cosmological SPH+N-body simulation to measure the alignment of cluster halos with their parent supercluster. For both the cluster halos and parent super-cluster they define the shape via the non-normalized inertia tensor. The find that strenght of the alignments increases with the degree of filamentarity of the supercluster.

The simulation has $2 \times 512^3$ particles in a box of side $500h^{-1}$Mpc . The dark matter particle mass is $6.6 \times 10^{10} h^{-1}\mathrm{M}_\odot$while for SPH particles is $1.2 \times 10^{10} h^{-1}\mathrm{M}_\odot$. The halo finding is done with a FOF algorithm with a linking length of 0.17 and keep objects with more than 100 partcles.

• (Lee & Pen 2002)Observational measurement for the alignment of galaxy spin axes with the local tidal shear field. For the measurement of shear, we have used the Point Source Catalog Redshift (PSCz) survey (a complete redshift survey from the IRAS Point Source Catalog) data. This was done down to a radial comoving distance of $\sim 150h^{-1}$Mpc .

• (Hatton & Ninin 2001) DM matter only simulation. $256^3$ particles, $100h^{-1}$Mpc , particle mass. Look for alignment of angular momentum vectors with neighbohring structures or other massive structures. They match halos using close pair statistics. They do not find any evidence for a

statistically significant mutual alignment of halos on any escale.

## REFERENCES


Aragón-Calvo M. A., van de Weygaert R., Jones B. J. T., van der Hulst J. M., 2007, ApJL, 655, L5

Basilakos S., Plionis M., Yepes G., Gottlöber S., Turchaninov V., 2006, MNRAS, 365, 539

Brunino R., Trujillo I., Pearce F. R., Thomas P. A., 2007, MNRAS, 375, 184

Codis S., Pichon C., Devriendt J., Slyz A., Pogosyan D., Dubois Y., Sousbie T., 2012, MNRAS, 427, 3320

Faltenbacher A., Li C., White S. D. M., Jing Y.-P., Shu-DeMao Wang J., 2009, Research in Astronomy and Astrophysics, 9, 41

Hahn O., Carollo C. M., Porciani C., Dekel A., 2007, MNRAS, 381, 41

Hatton S., Ninin S., 2001, MNRAS, 322, 576

Jones B. J. T., van de Weygaert R., Aragón-Calvo M. A., 2010, MNRAS, 408, 897

Laigle C., Pichon C., Codis S., Dubois Y., le Borgne D., Pogosyan D., Devriendt J., Peirani S., Prunet S., Rouberol S., Slyz A., Sousbie T., 2013, ArXiv e-prints

Lee J., Erdogdu P., 2007, ApJ, 671, 1248

Lee J., Kang X., Jing Y. P., 2005, ApJL, 629, L5

Lee J., Pen U.-L., 2002, ApJL, 567, L111

Libeskind N. I., Hoffman Y., Forero-Romero J., Gottlöber S., Knebe A., Steinmetz M., Klypin A., 2013, MNRAS, 428, 2489

Paz D. J., Stasyszyn F., Padilla N. D., 2008, MNRAS, 389, 1127

Platen E., van de Weygaert R., Jones B. J. T., 2008, MNRAS, 387, 128

Trowland H. E., Lewis G. F., Bland-Hawthorn J., 2013, ApJ, 762, 72

Zhang Y., Yang X., Faltenbacher A., Springel V., Lin W., Wang H., 2009, ApJ, 706, 747